

Protein translocation without specific quality control in a computational model of the Tat system

Chitra R Nayak¹, Aidan I Brown² and Andrew D Rutenberg²

¹Department of Physics, University of Toronto, Toronto, ON M5S 1A7, Canada

²Department of Physics and Atmospheric Science, Dalhousie University, Halifax, NS B3H 4R2, Canada

E-mail: rchitra.r@gmail.com and andrew.rutenberg@dal.ca


Received 5 April 2014, revised 28 June 2014

Accepted for publication 6 August 2014

Published 26 August 2014

Abstract

The twin-arginine translocation (Tat) system transports folded proteins of various sizes across both bacterial and plant thylakoid membranes. The membrane-associated TatA protein is an essential component of the Tat translocon, and a broad distribution of different sized TatA-clusters is observed in bacterial membranes. We assume that the size dynamics of TatA clusters are affected by substrate binding, unbinding, and translocation to associated TatBC clusters, where clusters with bound translocation substrates favour growth and those without associated substrates favour shrinkage. With a stochastic model of substrate binding and cluster dynamics, we numerically determine the TatA cluster size distribution. We include a proportion of targeted but non-translocatable (NT) substrates, with the simplifying hypothesis that the substrate translocatability does not directly affect cluster dynamical rate constants or substrate binding or unbinding rates. This amounts to a translocation model without specific quality control. Nevertheless, NT substrates will remain associated with TatA clusters until unbound and so will affect cluster sizes and translocation rates. We find that the number of larger TatA clusters depends on the NT fraction f . The translocation rate can be optimized by tuning the rate of spontaneous substrate unbinding, Γ_U . We present an analytically solvable three-state model of substrate translocation without cluster size dynamics that follows our computed translocation rates, and that is consistent with *in vitro* Tat-translocation data in the presence of NT substrates.

 Online supplementary data available from stacks.iop.org/pb/11/056005/mmedia

Keywords: twin-arginine translocation (Tat), substrate unbinding, quality control

(Some figures may appear in colour only in the online journal)

1. Introduction

Trafficking of biomolecules across membranes is an essential process for all living cells. The export of proteins is particularly interesting, and there are many distinct mechanisms for protein export from the bacterial cytoplasm [1]. Most of these mechanisms export linear peptide chains, which then fold outside the cytoplasm. Remarkably, the twin-arginine translocation (Tat) protein export pathway of bacteria, and the homologous Tat pathway of plant thylakoids, translocates folded proteins—often with cofactors—across energized membranes [2, 3]. With Tat-based export, proteins are not

dependent on extracytoplasmic conditions for folding, making the Tat system particularly important for bacterial virulence [4] and biotechnology applications [5].

Tat translocases [2, 3] consist of the TatA, TatB, and TatC proteins in the bacterial inner membrane. TatBC complexes recognize Tat signal peptides, while TatA multimers associate with TatBC complexes and are thought to form a transmembrane conduit. TatA complexes are large, dynamic, and broadly distributed in size [6, 7]. This is thought to allow the Tat system to accommodate a broad-range of folded substrate sizes (9–142 kDa substrates with approximately 2–7 nm diameter [8]).

Not every substrate with a targeting sequence is translocated. It is not known precisely what substrate properties determine translocatability, though goodness of fold for natural substrates [9–12] or moderate size and hydrophilicity for artificial substrates [13, 14] appear to be important. The distinction between translocatable and non-translocatable (NT) substrates can also be affected by suppressor mutations of the translocon apparatus [15]. How might the Tat translocon avoid blockage due to non-translocatable (NT) proteins and protein complexes? One possibility is that the Tat signal peptide only targets substrates to the translocon if they are well folded—so-called ‘proof-reading’ [16]. Such a mechanism might prevent NT substrates from binding to and blocking translocons. However, translocation of artificial substrates with long flexible linkers [17] as well as small unstructured substrates [14] has been reported. This implies that targeting of substrates to Tat translocons may not sensitively depend on the nature of the substrate. Indeed, non-translocatable substrates are observed to associate with the translocon [11, 18]. Nevertheless, translocatable [19] and NT [20, 21] substrates appear to only transiently associate with Tat translocons. This is consistent with the observation that degradation of misfolded Tat substrates appears to be independent of the Tat system [22].

The binding affinities or unbinding rates of targeted substrates may depend upon substrate properties, such as whether a particular substrate is well-folded or not. This is one form of the quality control hypothesis [9]. Lower binding affinities and/or higher unbinding rates would lead to lower translocation of targeted substrates, and presumably higher translocation of the remaining substrates. Nevertheless, this leaves open the question of whether any such quality control is needed to explain existing experimental phenomenology of the Tat system.

Accordingly, we explore the quality control null hypothesis—in which binding and unbinding rates of targeted substrates to the Tat translocon do not depend on substrate properties. To do this we develop a stochastic model of the binding and unbinding of protein substrates coupled with TatA cluster dynamics and substrate translocation. We allow a bound substrate to translocate when sufficient TatA are present in a cluster. To allow TatA clusters to dynamically adjust to different substrate sizes, we additionally allow the TatA cluster dynamics to depend on the binding status of the cluster: with a bound substrate, growth of the cluster is favoured, and without a bound substrate, shrinkage is favoured; such behaviour is similar to TatA behaviour seen *in vivo* [11]. This also reflects the experimental observation that the TatA oligomerization process is induced by the substrate and this is reversed only once the substrate unbinds or translocates [23]. Consistent with our quality control null hypothesis, we also assume that cluster dynamics do not depend on substrate properties. With our model, both the TatA cluster size distribution and substrate translocation rates are computationally investigated. The model allows the optimization of the translocation efficiency of multiple Tat translocases as the fraction f of NT substrates is varied. We find that significant translocation is possible with the non-

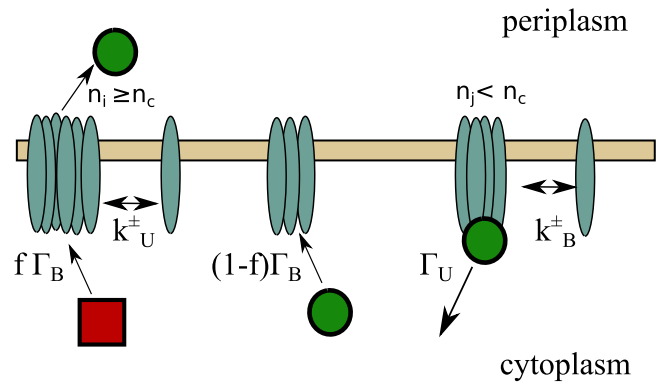


Figure 1. Illustration of our model dynamics. Membrane associated TatA (blue-grey ellipses) are in three clusters together with two monomers from n_{pool} . Substrates can associate with clusters at rate Γ_B , and are either translocatable (green circles, fraction $1 - f$) or non-translocatable (NT red square, fraction f). Translocatable substrates are translocated into the periplasm when the cluster size n_i equals or exceeds a threshold n_c . Substrates disassociate from clusters back into the cytoplasm at rate Γ_U , and this same disassociation rate applies both to translocatable substrates with $n_i < n_c$ and to NT substrates. Clusters grow by a monomer at rate $k^+ n_{\text{pool}}$ or shrink at rate k^- , and these rates depend on whether the cluster is unassociated (‘U’) or bound (‘B’) to a substrate. There are N clusters, and n_{tot} TatA molecules that include both those in clusters and those in n_{pool} . TatBC is not shown, but is implicitly part of each cluster to allow substrate association.

specific substrate disassociation rate. The model also recovers a notable large-size tail that was observed in high-resolution *in situ* fluorescence studies of TatA clusters [6], which we ascribe to transiently stalled translocases. In addition, we develop an analytical three-state model without TatA cluster dynamics. This three-state model provides a reasonable approximation of our full stochastic results, and is consistent with *in vitro* translocation data of mixed translocatable and NT substrates [20].

2. Model

We assume a fixed number N of oligomeric TatA translocation complexes (or ‘clusters’), and a fixed total number n_{tot} of TatA molecules in the membrane. At a given time t , the i th oligomeric TatA cluster is comprised of n_i monomers. TatA monomers that are not in clusters form a common monomeric pool, where $n_{\text{pool}} = n_{\text{tot}} - \sum_{i=1}^N n_i$. We note that TatBC clusters (see e.g. [24]) are implicit in our model, and are necessary for substrate binding, unbinding, and translocation.

The model dynamics are illustrated in figure 1. Each TatA cluster may be either associated with a translocation substrate, or not. A substrate has a Tat targeting sequence, or is a complex of molecules associated with a protein with a targeting sequence [2]. Association of substrates to empty clusters occurs at rate Γ_B , but a fraction f of those substrates are NT. Non-specific unbinding of substrates occurs at a rate Γ_U , which allows for unblocking of clusters bound to NT substrates but also causes premature release of translocatable substrates. The values of Γ_B and Γ_U are discussed in section 4.

Following our quality control null hypothesis, we assume that the rates Γ_B and Γ_U do not depend on whether the substrate is translocatable or NT, nor on any non-specific interactions between substrates and the Tat translocon. While the details of the signal peptide can affect translocation rates [21, 25, 26], we assume for simplicity that all of our substrates have the same signal peptides.

Bound translocatable substrates are translocated when their associated cluster is equal to or larger than a critical size n_c . For oligomeric substrates [27], n_c would reflect the oligomer size. NT substrates are those that do not translocate regardless of cluster size, whether due to misfolding, substrate size, or other substrate properties.

Clusters grow by one monomer at a rate $k^+ n_{\text{pool}}$, where n_{pool} is the number of monomers not associated with any cluster, and shrink by one monomer at a rate k^- . We assume that there are distinct rates for complexes with bound substrates (k_B^\pm) and those without (k_U^\pm). These distinct rates lead to a more dynamic system of growing and shrinking clusters, and allows large substrates to be temporarily accommodated through cluster growth, consistent with TatA recruitment to functionally engaged Tat translocons [11, 23]. Because substrates primarily interact with TatB and TatC [24, 28], we expect that TatBC modulates TatA cluster growth and so assume that the rates k^\pm are independent of cluster size compared to the differences between k_U^\pm and k_B^\pm . Following our quality control null hypothesis, we also assume that the cluster rates k^\pm do not vary across substrates.

Very little is known about effective rate constants for cluster growth. All of our rates (k 's and Γ 's) are dimensionless; and we generally work in units of the binding rate so that $\Gamma_B = 1$. Unless otherwise indicated, we use $k_B^+ = 0.05$, $k_B^- = 1.5$, $k_U^+ = 0.005$, and $k_U^- = 7.0$, where we have $k_B^+ > k_U^+$ and $k_B^- < k_U^-$ so that substrate-associated clusters grow faster and shrink more slowly than unbound clusters. The values for the parameters k^\pm are chosen to allow growth and shrinkage of clusters to occur quickly enough to reach n_c , but not so rapidly that binding and cluster dynamics are on different timescales. These rates were found to give a cluster size distribution that is qualitatively similar to what is seen experimentally (see below). We systematically vary both the unbinding rate Γ_U and the NT fraction f . Variation of the parameter values k^\pm is explored in the supplemental materials.

The Gillespie algorithm [29] was used to perform fully stochastic simulations of cluster growth and shrinkage, together with substrate binding, unbinding, and translocation. Clusters were allowed to reach a steady-state distribution before the time-averaged translocation rate R and distribution of cluster sizes $P(n)$ were measured. Experimental studies of fluorescently labelled TatA indicate that there are $N = 15 \pm 9$ TatA clusters per bacterial cell, with approximately $n_{\text{tot}} \approx 560$ TatA molecules per cell and $n_{\text{pool}} \approx 100$ TatA that are not associated with complexes [6]. Correspondingly, unless otherwise noted we take the number of clusters $N = 15$ and the number of monomers $n_{\text{tot}} = 560$.

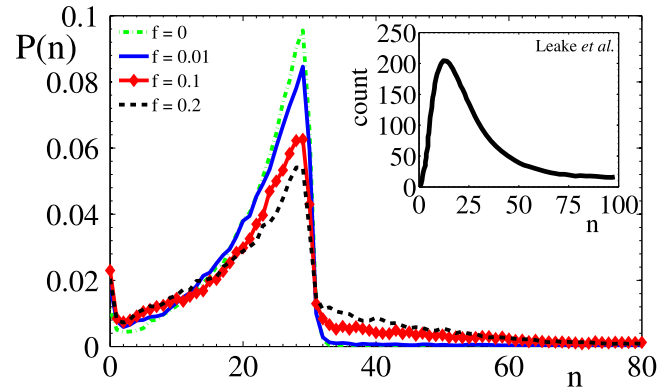


Figure 2. The cluster size distribution. The cluster size distribution $P(n)$ versus cluster size n for a variety of NT fractions f with $n_{\text{tot}} = 560$ and $N = 15$. We use $\Gamma_U = 0.5$ and a single threshold size for translocation $n_c = 30$. A prominent peak is seen at n_c , since unassociated clusters tend to shrink after translocation because $k_U^- > k_B^-$ and $k_U^+ < k_B^+$. As f increases, a significant tail grows above n_c due to growth of clusters with associated NT substrates. The inset shows the experimental distribution of TatA clusters digitized from figure 4I of Leake *et al* [6]. The parameter values of this figure, together with $\Gamma_B = 1$, $\Gamma_U = 0.5$, $k_B^+ = 0.05$, $k_B^- = 1.5$, $k_U^+ = 0.005$, and $k_U^- = 7.0$, also apply to other figures unless otherwise noted.

3. Results

3.1. Cluster size

The model cluster size distributions plotted in figure 2, of $P(n)$ versus the cluster size n , exhibit some of the qualitative features seen in the experimental distribution of TatA cluster sizes reported by Leake *et al* [6] and shown in the inset: an increase from arbitrarily small clusters, a distinct peak, and an extended tail for larger cluster sizes.

As shown in figure 2, increasing the NT fraction f increases the magnitude of the tail of $P(n)$ for $n > n_c$. Clusters with bound substrates will tend to grow, due to larger k_B^+ and smaller k_B^- . Clusters with bound NT substrates do not translocate at n_c , so growth of individual clusters beyond n_c will be limited by the unbinding rate Γ_U (see figure S1). Additionally, depletion of the TatA monomer pool generally limits cluster growth. Systematically larger tails for $P(n)$ are seen with more rapid bound growth k_B^+ (see figure S2), and with smaller unbound decay k_U^- (see figure S3). Interestingly, $P(n)$ is also affected by changes in Γ_B (see figure S1). Larger Γ_B allows rapid rebinding of substrates to large clusters, which prevents their relaxation and leads to a larger tail for $n > n_c$ and less weight for $n < n_c$.

In addition to the tail of $P(n)$ for $n > n_c$, the location of the peak of $P(n)$ in the model is approximately determined by n_c . A variety of Tat substrates [2], with a range of sizes and abundances, would be expected to round the sharp peak obtained with the model using a single value of n_c and lead to better qualitative agreement with the rounded experimental distribution of TatA cluster sizes [6] shown in the inset of figure 2. To explore this effect in figure 3, for each substrate we have selected n_c from a truncated Gaussian distribution with standard deviation σ , truncated at 2σ with an average

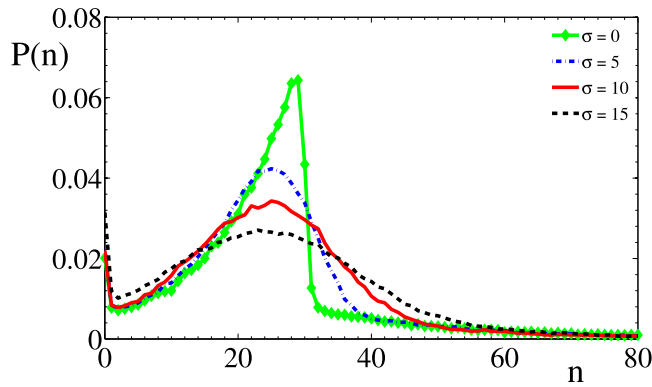


Figure 3. Cluster size distribution with a distribution of substrate sizes. $P(n)$ versus cluster size n for different distributions of the substrate sizes n_c . All substrate size distributions are Gaussian distributions with mean $\langle n_c \rangle = 30$, truncated at 2σ . In all cases $f = 0.1$, so $\sigma = 0$ (green diamonds) is the same as the red diamonds in figure 2. Other parameter values are the same as in figure 2.

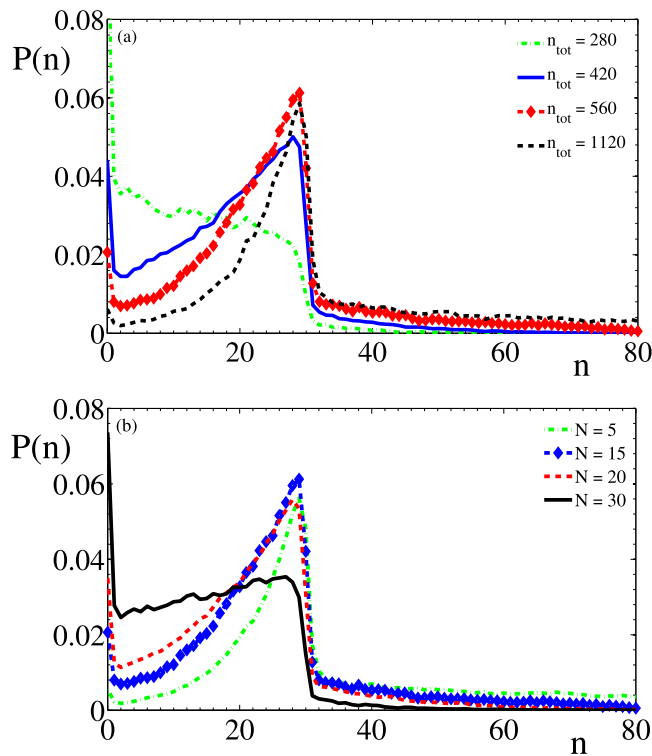


Figure 4. Cluster size distribution as number of clusters or number of TatA are varied. (a) Cluster size distribution $P(n)$ versus n for $N = 15$ clusters with variable n_{tot} . (b) As previous, but with $n_{\text{tot}} = 560$ and variable N . For both figures we use $f = 0.1$. Other parameter values are as given in figure 2.

$\langle n_c \rangle = 30$. We see that using a distribution of n_c rounds the peak of the cluster size distribution $P(n)$ but does not significantly change the behaviour for $n < n_c$. Since we are using a single value of n_c for the rest of this paper, we have chosen $n_c = 30$ to better emphasize the $n > n_c$ tail of $P(n)$.

In figure 4 we show how the cluster size distribution $P(n)$ changes as (a) the number of TatA monomers n_{tot} or (b) the number of translocons N is changed. For the smallest $n_{\text{tot}} = 280$ the peak near n_c is lost. For larger $n_{\text{tot}} \gtrsim 420$ the

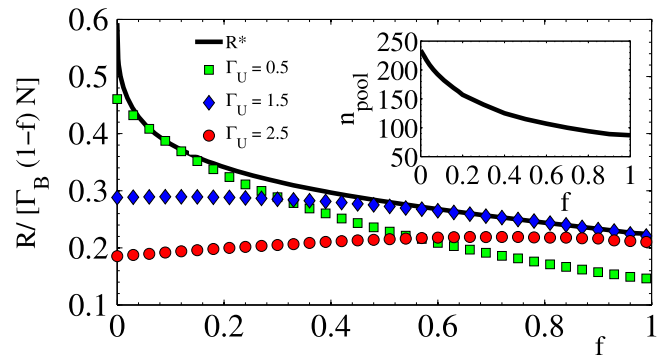


Figure 5. Scaled translocation rate as NT fraction is varied. Scaled translocation rate per cluster $R/(\Gamma_B(1-f)N)$ versus the NT fraction f for $n_{\text{tot}} = 560$ and $N = 15$. Shown are different unbinding rates Γ_U . Other parameter values are as given in figure 2. The thick black line is the scaled optimal translocation rate R^* , where for each value of f we have chosen the $\Gamma_U = \Gamma_U^*(f)$ that maximizes R . The inset shows the average size of the monomeric pool, n_{pool} versus f , corresponding to the maximal R^* line.

distribution at small n retains a similar shape with increasing n_{tot} , but decreases in magnitude as n_{tot} increases. In contrast, the large- n tail increases with n_{tot} . As shown in figure 4(b), we see corresponding effects when N is varied at fixed n_{tot} , with similar monomer numbers per translocon, n_{tot}/N , leading to qualitatively similar cluster size distributions.

3.2. Translocation rate

The total translocation rate R can be no more than $N\Gamma_B(1-f)$ —the binding rate of translocatable substrates to N empty clusters. In figure 5, we show the scaled translocation rate per cluster, $R/(\Gamma_B(1-f)N)$, versus the NT fraction f for $n_{\text{tot}} = 560$ and $N = 15$. As expected, scaled translocation rates are below the theoretical limit of 1 for all NT fractions f . This is because, as illustrated in figure 2, most clusters are smaller than n_c —and so need to grow before they can translocate bound substrates. Translocation is further reduced by bound NT substrates, which must be disassociated before further substrate binding and translocation is possible. We show three scaled translocation rates, for $\Gamma_U = 0.5, 1.5$, and 2.5 (green squares, blue diamonds, and red circles, respectively). We see that despite no specific quality control mechanism, translocation rates of 50% of the theoretical maximum are possible at smaller f while even at large f translocation rates can still reach 20% of the theoretical maximum.

From the change in the translocation rate dependence on f between the different Γ_U values in figure 5, we see that for smaller values of f a smaller Γ_U leads to higher scaled translocation rates while at larger values of f a larger Γ_U leads to more translocation. More generally, we find that there is an optimal Γ_U^* that leads to the highest translocation rate R^* for each value of the NT fraction f . If $\Gamma_U < \Gamma_U^*$, then too many NT substrates block translocation. If $\Gamma_U > \Gamma_U^*$, then too many translocatable substrates are removed before the cluster size reaches n_c . We numerically identify Γ_U^* by varying Γ_U and measuring R , as f is varied. The corresponding optimal

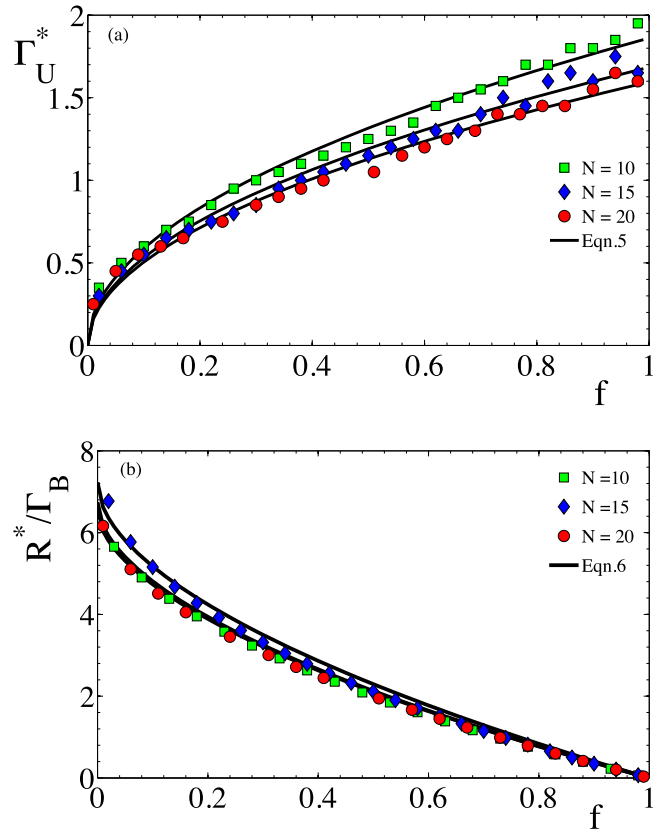


Figure 6. Optimized translocation as NT fraction is varied. (a) The optimal unbinding rate, Γ_U^* , that maximizes the translocation rate versus the NT fraction f . For a fixed number of TatA, $n_{\text{tot}} = 560$, results are shown for different numbers of clusters N as indicated by the legend. Other parameter values are as given in figure 2. All curves show a characteristic square-root dependence on f , as shown by the phenomenological fits to a simplified three-state model of translocation from equation (5) (black lines). (b) The corresponding scaled total translocation rates R^*/Γ_B versus f , together with phenomenological fits (black lines) to equation (6).

translocation rate R^* is plotted with a solid black line in figure 5. The curves for specific values of Γ_U in figure 5 demonstrate that close to optimal translocation can be obtained for a wide range of f for each value of Γ_U . The relationship between Γ_U^* and f is shown in figure 6(a).

We also note that there is a decreasing monomeric pool of TatA with increasing f , as shown in the inset of figure 5 and reflecting the increased tail of $P(n)$ with f shown in figure 2. Our observed range of $n_{\text{pool}} \sim 100$ – 200 is comparable to $n_{\text{pool}} \approx 100$ reported experimentally [6].

3.3. Optimal number of clusters N

In figure 6(a), the optimal Γ_U versus f is investigated for different number of clusters N . The optimal Γ_U^* depends strongly on f but only weakly on N , and a similar weak dependence is seen in figure 6(b) for the corresponding optimal scaled total translocation rates R^*/Γ_B . Nevertheless, we can see that R^* does not monotonically increase with N , but is slightly larger for $N = 15$ (blue diamonds). This is

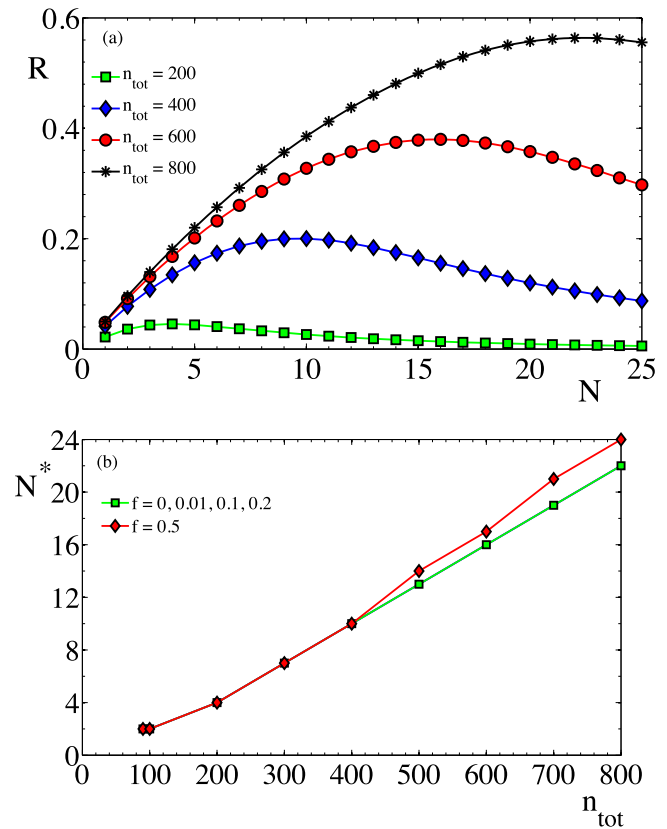


Figure 7. Translocation as the number of clusters is varied. (a) The total translocation rate, R , versus number of clusters N for variable total number of monomers n_{tot} . The NT fraction $f = 0.1$. (b) The number of clusters that maximizes translocation, N^* , versus n_{tot} for different NT fractions f . The green squares have four superimposed curves. Other parameter values are as given in figure 2.

explored in more detail in figure 7(a), where the total translocation rate R is plotted versus number of clusters N for different total number of TatA, n_{tot} , as indicated by the legend. For each n_{tot} there is an optimal N^* that maximizes the total translocation rate R . This behaviour arises because the clusters share the same fixed number n_{tot} of TatA, forcing a tradeoff between cluster size and cluster number. A smaller N has a reduced total translocation rate, because n_{pool} is sufficiently large for translocation to be limited by Γ_B , while a larger N will slow the cluster growth needed to translocate at size n_c due to the depletion of n_{pool} .

Figure 7(b) shows that the optimal N^* increases with n_{tot} . For $n_{\text{tot}} \gtrsim 200$, the optimal number of clusters N^* scales approximately linearly with larger values of n_{tot} . We also see that N^* is not strongly dependent on the NT fraction. Together, this implies that stoichiometric control of cluster number may be sufficient to maintain close to optimal translocation rates in the face of varying levels of TatA.

We can now reconsider how the cluster size distribution $P(n)$ depends upon N , as shown in figure 4(b). With the chosen parameter values the optimal number of clusters is $N^* = 15$. For $N \lesssim N^*$, increasing N slightly decreases the tail at larger n due to the availability of monomers, and moderately increases the distribution of smaller n . However, once

$N > N^*$ we see a qualitatively different distribution with a significant number of very small clusters. In comparison with the experimental $P(n)$ (see inset of figure 2) we see that our model gives similar results if $N \lesssim N^*$ —both have few small clusters and an increase to a distinct peak, rather than a larger population of smaller clusters. The model parameters are underconstrained by the current experimental data, and we have chosen kinetic rates so that $N^* = 15$ is similar to the number of TatA clusters observed *in vivo* [6] and equal to our default value of N . Nevertheless, we can say that results are consistent with the Tat system having close to an optimal number of translocons given the amount of TatA.

3.4. Three-state model

To better understand our translocation rates, we consider a simplified stochastic three-state Tat translocation model. The three states, with corresponding probabilities, are empty (p_0), bound with translocatable substrate (p_B), and bound with non-translocatable substrate ($p_{NT} = 1 - p_0 - p_B$). Two transition rates that directly correspond to the full model are Γ_B , the rate at which substrates bind to an empty cluster, and Γ_U , the rate at which substrates unbind from a cluster without translocation. We add one additional rate, Γ_T , the translocation rate of translocatable substrates, to phenomenologically account for cluster size dynamics, threshold size n_c , as well as the mechanics of translocation. Our dynamical equations are then

$$\frac{dp_0}{dt} = \Gamma_U p_{NT} + (\Gamma_U + \Gamma_T) p_B - \Gamma_B p_0, \quad (1)$$

$$\frac{dp_B}{dt} = (1 - f) \Gamma_B p_0 - (\Gamma_U + \Gamma_T) p_B, \quad (2)$$

$$\frac{dp_{NT}}{dt} = f \Gamma_B p_0 - \Gamma_U p_{NT}, \quad (3)$$

where f is the fraction of non-translocatable substrates. We use $p_0 + p_B + p_{NT} = 1$ to solve these equations in steady state, where the time-derivatives vanish, and obtain

$$p_B = \frac{(1 - f) \Gamma_B \Gamma_U}{f \Gamma_B \Gamma_T + \Gamma_U (\Gamma_B + \Gamma_T + \Gamma_U)}, \quad (4)$$

and a corresponding translocation rate $R = N_{\text{eff}} \Gamma_T p_B$, where N_{eff} is the effective number of independent clusters participating in translocation. Note that our three-state model mathematically corresponds to a special case of a ‘one site’ model of an always-open transport channel developed by Zilman *et al* [30], where their $J_n = (1 - f) \Gamma_B$, $J_m = f \Gamma_B$, $r_m^{\text{right}} = 0$, $r_m^{\text{left}} = r_n^{\text{left}} = \Gamma_U$, and $r_n^{\text{right}} = \Gamma_T$.

To compare with optimized translocation results in figure 6, we maximize the translocation rate with respect to the unbinding rate Γ_U , with $\partial R / \partial \Gamma_U = 0$, and obtain

$$\Gamma_U^* = \sqrt{\Gamma_T \Gamma_B f}, \quad (5)$$

$$R^* = \frac{N_{\text{eff}} \Gamma_T \Gamma_B (1 - f)}{\left[\Gamma_B (1 - f) + \left(\sqrt{\Gamma_T} + \sqrt{\Gamma_B f} \right)^2 \right]}. \quad (6)$$

N_{eff} is the effective number of independent clusters participating in translocation, so that we expect $N_{\text{eff}} \lesssim N$. As shown by the solid black lines in figure 6(a), the characteristic square-root dependence of Γ_U^* versus f from equation (6) describes the full model results well. Fit by eye, we find that $\Gamma_T = 3.5, 2.8$, and 2.5 for $N = 10, 15$, and 20 respectively. The phenomenological translocation rate for each cluster, Γ_T , decreases with increasing N —as expected since n_{pool} decreases with increasing N . As shown by the solid black lines in figure 6(b), equation (6) also provides a satisfactory fit for the optimal translocation rates. Using the Γ_T values, we fit by eye to find $N_{\text{eff}} = 6.2, 7.0$, and 6.4 , for $N = 10, 15$, and 20 , respectively. $N_{\text{eff}} < N$, as expected. Interestingly, we see that N_{eff} is largest for $N = 15$, where $N \simeq N^*$. Note that the values of Γ_T and N_{eff} will depend on the kinetic parameters (k^\pm) of the full model.

Our three-state model does not include any cluster size dynamics, so is largely independent of our detailed assumptions of cluster size dynamics. Additionally, it appears to be a reasonable approximation of our full dynamical model. The three-state model is also easily adapted to different experimental protocols.

Our models parameterize the non-translocatable fraction f independently from the substrate binding rate Γ_B ; this highlights the role of f in determining an optimal Γ_U . *In vitro*, it can be more convenient to independently adjust the bulk substrate concentrations, ρ_T and ρ_{NT} of translocatable and NT substrates, respectively. For our parameters, this then gives

$$\Gamma_B = \gamma_T \rho_T + \gamma_{NT} \rho_{NT} \quad (7)$$

$$f = \frac{1}{1 + \rho_T / \rho_{NT}}. \quad (8)$$

We have allowed for distinct binding constants γ_T and γ_{NT} for translocatable and NT substrates, respectively, to allow for quantitative effects of substrate size in affecting diffusion-limited association rates [31]. We will continue to assume that unbinding Γ_U is the same for both substrates.

Musser and Theg quantitatively characterized translocation in a thylakoid Tat system [20]. They considered radioactively labelled ($\rho_R = 100$ nM) and unlabelled (ρ_{NR}) fractions of a translocatable substrate, so that $\rho_T = \rho_R + \rho_{NR}$ and $\rho_{NT} = 0$. Then the total translocation amount of labelled substrate in time Δt is $R_{\text{tot},R} = R \Delta t \rho_R / \rho_T$, i.e.

$$R_{\text{tot},R} = \frac{\gamma_T \rho_R \Gamma_T N_{\text{eff}} \Delta t}{\gamma_T (\rho_R + \rho_{NR}) + \Gamma_U + \Gamma_T}, \quad (9)$$

where we have used our unoptimized three-state model with a phenomenological translocation rate Γ_T and $f = 0$.

Musser and Theg then repeated their experiment with a non-translocatable (biotinylated) unlabelled substrate concentration $\rho_{NT} = \rho_{NR}$, and the same translocatable labelled concentration so that $\rho_T = \rho_R$. We then have a total

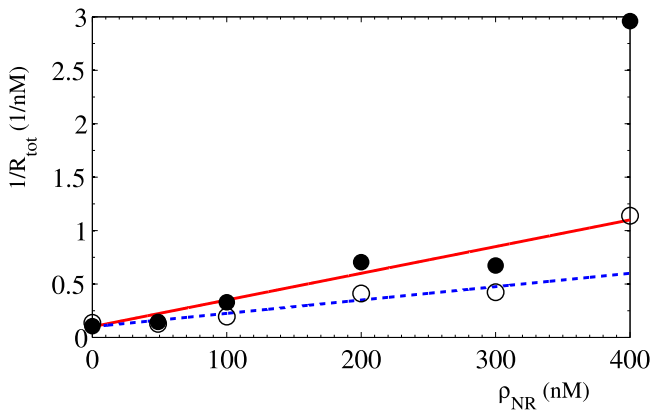


Figure 8. *In vitro* translocation data analyzed with simplified three-state model. The inverse total translocation versus unlabelled biotinylated substrate concentration ρ_{NR} from figure 3E of Musser and Theg [20]. All points have $\rho_R = 100$ nM. The open and closed circles correspond to experiments done with avidin (where $\rho_{NT} = \rho_{NR}$, and equation (10) is applicable) or without (where $\rho_{NT} = 0$, so that equation (9) is applicable), respectively. We have shown linear fits by eye to equations (9) or (10) with solid red or dashed blue lines, respectively. We have imposed a common y-intercept on our fits, corresponding to the translocation of radioactively labelled substrate ρ_R that remains the same between the two experiments.

translocation amount of labelled substrate

$$R_{tot,T} = \frac{\gamma_T \rho_R \Gamma_T N_{eff} \Delta t}{\gamma_T \rho_R + \gamma_{NT} \rho_{NR} + \Gamma_U + \Gamma_T + \gamma_{NT} \rho_{NR} \Gamma_T / \Gamma_U}, \quad (10)$$

with an additional term in the denominator due to γ_{NT} . We see that R_{tot}^{-1} in both equations (9) and (10) depends linearly on the unlabelled concentration ρ_{NR} .

In figure 8, we have plotted the inverse total translocation amount R_{tot}^{-1} versus the concentration of unlabelled substrate ρ_{NR} using digitized experimental data from figure 3E of [20]. The expected linear behavior of R_{tot}^{-1} versus ρ_{NR} is apparent at larger values of R_{tot} (i.e. smaller values of ρ_{NR}), where systematic and statistical errors should be less significant. In that regime, our three-state model appears consistent with the experimental translocation data both with and without NT substrates.

4. Discussion and conclusions

The Tat protein export pathway translocates folded proteins across membranes in bacteria and plant cells [2, 3], and Tat translocons must accommodate a range of substrate sizes while staying unclogged by NT substrates. Our model demonstrates how a non-specific substrate unbinding rate (Γ_U) can recover an appreciable fraction of the maximal translocation rate achievable with no NT substrates (see figure 5). Non-specific substrate unbinding still kinetically discriminates [32] between translocatable and NT substrates, since the former are often translocated before unbinding can occur.

Association and disassociation rates of one substrate with the Tat translocation complex have recently been estimated *in vitro* by Whitaker *et al* [19] with bacterial extracts. They found $\Gamma_U \approx 0.042$ s⁻¹ (their k_{off}) and $\Gamma_B = k_{on} \rho_{substrate}$, where $k_{on} \approx 10^6 - 10^7$ M⁻¹ s⁻¹ [19]. (This binding may occur via a membrane-associated intermediate [21].) Given a bacterial volume of $1 \mu\text{m}^3$, substrate numbers of $1-10^4$ per cell would give $\Gamma_B \approx 10^{-3}/\text{s} - 10^2/\text{s}$ per distinct substrate. Given the number of different Tat substrates in the cell [2], it appears that $\Gamma_U \lesssim \Gamma_B$ is typical for, e.g., *Escherichia coli*, but $\Gamma_U \gtrsim \Gamma_B$ may be accessible in, e.g., model vesicular systems with few translocation substrates. We see from figure 6(a) that $\Gamma_U \lesssim \Gamma_B$ (where $\Gamma_B = 1$), is consistent with optimized translocation for NT fractions $f \lesssim 0.2$.

We have also explored optimization of the number of clusters N as the number of TatA molecules in the membrane n_{tot} is varied. The number of clusters has an optimal value, N^* , which maximizes the translocation rate corresponding to a given number of TatA molecules. For $n_{tot} = 560$ monomers, $N^* \approx 15$, which leaves a pool of monomers $n_{pool} \approx 100$. These optimal values are consistent with *in vivo* studies of the Tat system [6]. We also find that if the number of clusters is much more than N^* then the distinctive peak of the cluster size distribution seen in figure 2, and reported experimentally by Leake *et al* [6], is lost (see solid black curve in figure 4(b)). Together this indicates that N could be close to optimal in the bacterial Tat system. It would be interesting to explore how, and how well, optimal behaviour is achieved *in vivo* as f and n_{tot} are varied.

Our full model, with cluster size dynamics that depend on whether substrates are bound or not, recovers the qualitative shape and distinctive long tail of large TatA clusters reported by Leake *et al* [6]. Our model is a quantitative ‘bespoke channel model’ [2], in which the cluster size n_i dynamically accommodates the substrate size n_c so that translocation can occur. We note however that both $n_i > n_c$ and $n_i < n_c$ are observed in our model, the former as a result of recent interactions of the cluster with larger or NT substrates, and the latter as a result of assembly after recent binding and disassembly after unbinding. We also observe significant variability of our cluster distribution $P(n)$ with number of clusters N and with number of monomers n_{tot} . This indicates caution must be taken in interpreting how cluster sizes observed through, e.g., cross-linking studies [33] or fluorescence microscopy [6], respond to substrate sizes. We also note that substrate shape can affect both the critical cluster size n_c and the effective translocation rate Γ_T [34]. We find that the cluster size distribution is broadened by a distribution of the critical size n_c (see figure 3). The cluster size n_c necessary for translocation may also have a nonlinear dependence on substrate radius. However, we do find that the peak of $P(n)$ is always near n_c —so studies of Tat translocation in a thylakoid system that allows for a single translocation substrate (see e.g. [20] or [33]) but with fluorescently labelled TatA (see e.g. [6]) that resolves the full cluster size distribution should be able to determine how TatA cluster sizes respond to substrate size.

There are many dynamical processes that could couple TatA complex size with substrate translocation; we have implemented a relatively simple one with k^\pm . The current picture appears to be that TatBC complexes, with perhaps some TatA, associate with substrates and then recruit more TatA. Substrates appear to associate at the side of TatBC complexes [24], which could allow for discrimination between bound k_B^\pm and unbound k_U^\pm rates [23]. TatA association with substrate-associated TatBC complexes may happen through recruiting TatA tetramers [6], perhaps after initial recruitment of larger TatA complexes (see, e.g., [35]). Smaller monomer or tetramer association after initial complex recruitment would be consistent with our model, though association of larger TatA complexes at later stages would probably change our cluster size distribution significantly. Nevertheless, our simplified three-state translocation model, with substrate unbinding but without cluster dynamics, appears to fit translocation data with a variable fraction of labelled substrates [20]. We believe that as long as both translocation and cluster size dynamics are fast compared to Γ_U , the translocon can kinetically discriminate [32] between translocatable and non-translocatable substrates.

Absolute translocation rates have been measured *in vitro* with plant thylakoids, and Alder and Theg [36] report $v_{\max} = 6.2/(\text{thylakoid} \cdot \text{s})$ and $K_m = 189 \text{ nM}$. With approximately 15000 translocons per chloroplast [37] and approximately 500 thylakoids per chloroplast [38], we estimate $N_{\text{eff}} \approx 30$. Comparing with equation (9) with $f = 0$ we obtain $v_{\max} = \Gamma_T N_{\text{eff}}$ and $K_M = (\Gamma_U + \Gamma_T)/\gamma$, which then gives $\Gamma_T \approx 0.2/\text{s}$ (assuming $\Gamma_U \ll \Gamma_T$) and $\gamma = 10^6 \text{ M}^{-1} \text{ s}^{-1}$. This γ is in remarkable agreement with the results of Whitaker *et al* [19], and indicates that Tat kinetics may be similar in the thylakoid and bacterial systems. While this $\Gamma_T \approx 0.2/\text{s}$ is much faster than $\Gamma_U \approx 0.042/\text{s}$ [19], it is somewhat less than the Γ_B expected for the more abundant bacterial Tat substrates. This indicates that the most abundant substrates may be rate limited by translocation timing, which includes TatA cluster dynamics, rather than by association or stalled translocons due to NT substrates.

We do not speculate about the mechanics of a substrate actually crossing the membrane or how a threshold number of TatA would allow translocation for a substrate of a given size. With respect to translocation, the simple assumptions made are that translocation can occur for a translocatable substrate once a sufficient number of TatA monomers have accumulated, and that the translocation process is rapid compared to the timescales of TatA and substrate binding and unbinding. We focus on the role of an unbinding rate to avoid clogging the Tat translocon and how non-translocatable substrates could affect the translocation of other substrates through the availability of TatA monomers.

We have mostly considered both binding Γ_B and unbinding Γ_U to be independent of the substrate, and in particular of whether the substrate is translocatable or NT. But, experimental studies have shown that variations of the signal peptides can affect translocation rates [21, 25, 26] and that folding or lack of folding can affect signal peptide binding [11]. Within our model this could arise from variations of Γ_B ,

or of Γ_U , or of both. Indeed, to best agree with *in vitro* translocation studies of Musser and Theg [20] in section 3.4 we have allowed Γ_B to reflect different size substrates. Clearly some substrate dependence of at least Γ_B is indicated, and diffusion-limited rates will depend somewhat on the folded nature of the substrate. Substrate dependence of Γ_B and Γ_U , or of cluster-size dynamics through k^\pm , are straight-forward to include in our model. Nevertheless, little is known about any such substrate-dependent kinetics, and so we have not attempted to characterize them in our model.

If and how quality control [9] of Tat translocation is achieved is being actively investigated: chaperones can affect Tat substrate binding [39]; unstructured proteins [14] and small, unfolded, hydrophilic polypeptides [40] can be translocated by Tat; and mutations in the Tat system can enable it to translocate previously untranslocatable proteins [15]. These studies focus on what defines non-translocatable (NT) substrates, while we focus on how reversible substrate association (via Γ_U) can lead to a significant fraction of the maximal translocation rate being achieved—see figure 5. We have shown that the optimal unbinding rate depends on the NT fraction f . *In vivo*, with a variety of substrates, each with its own abundance and NT fraction, we expect that translocation could be further controlled with substrate-dependent association and unbinding rates. This would amount to specific but passive quality control, and might be implemented in part through variations of associated signal peptides [21, 25, 26]. A functional definition of ‘non-translocatable’ may also depend upon the speed of translocation with respect to the unbinding rate. It would be interesting to measure substrate unbinding rates in suppressor mutants of Tat translocation that allow previously NT substrates to significantly translocate [15].

Acknowledgments

We thank the Natural Science and Engineering Research Council (NSERC) for operating grant support, and the Atlantic Computational Excellence Network (ACEnet) for computational resources. CRN thanks ACEnet for fellowship support. AIB thanks NSERC, ACEnet, the Sumner Foundation, and the Killam Trusts for fellowship support.

References

- [1] Economou A, Christie P J, Fernandez R C, Palmer T, Plano G V and Pugsley A P 2006 Secretion by numbers: protein traffic in prokaryotes *Mol. Microbiol.* **62** 308–19
- [2] Palmer T and Berks B C 2012 The twin-arginine translocation (Tat) protein export pathway *Nat. Rev. Microbiol.* **10** 483–96
- [3] Fröbel J, Rose P and Müller M 2012 Twin-arginine-dependent translocation of folded proteins *Phil. Trans. R. Soc. London B* **367** 1029–46
- [4] De Buck E, Lammertyn E and Anne J 2008 The importance of the twin-arginine translocation pathway for bacterial virulence *Trends Microbiol.* **16** 442–53

- [5] Brüser T 2007 The twin-arginine translocation system and its capability for protein secretion in biotechnological protein production *Appl. Microbiol. Biotechnol.* **76** 35–45
- [6] Leake M C, Greene N P, Godun R M, Granjon T, Buchanan G, Chen S, Berry R M, Palmer T and Berks B C 2008 Variable stoichiometry of the TatA component of the twin-arginine protein transport system observed by *in vivo* single-molecule imaging *Proc. Natl. Acad. Sci. USA* **105** 15376–81
- [7] Gohlke U, Pullan L, McDevitt C A, Porcelli I, de Leeuw E, Palmer T, Saibil H R and Berks B C 2005 The TatA component of the twin-arginine protein transport system forms channel complexes of variable diameter *Proc. Natl. Acad. Sci. USA* **102** 10482–6
- [8] Berks B C, Sargent F and Palmer T 2000 The Tat protein export pathway *Mol. Microbiol.* **35** 260–74
- [9] DeLisa M P, Tullman D and Georgiou G 2003 Folding quality control in the export of proteins by the bacterial twin-arginine translocation pathway *Proc. Natl. Acad. Sci. USA* **100** 6115–20
- [10] Matos C F R O, Robinson C and di Cola A 2008 The Tat system proofreads FeS protein substrates and directly initiates the disposal of rejected molecules *EMBO J.* **27** 2055–63
- [11] Panahandeh S, Maurer C, Moser M, DeLisa M P and Müller M 2008 Following the path of a twin-arginine precursor along the TatABC translocase of *Escherichia coli* *J. Biol. Chem.* **283** 33267–75
- [12] Maurer C, Panahandeh S, Moser M and Müller M 2009 Impairment of twin-arginine-dependent export by seemingly small alterations of substrate conformation *FEBS Lett.* **583** 2849–53
- [13] Cline K and McCaffery M 2007 Evidence for a dynamic and transient pathway through the TAT protein transport machinery *EMBO J.* **26** 3039–49
- [14] Richter S, Lindenstrauß U, Lucke C, Bayliss R and Brüser T 2007 Functional Tat transport of unstructured, small, hydrophilic proteins *J. Biol. Chem.* **282** 33257–64
- [15] Rocco M A, Waraho-Zhmayev D and DeLisa M P 2012 Twin-arginine translocase mutations that suppress folding quality control and permit export of misfolded substrate proteins *Proc. Natl. Acad. Sci. USA* **109** 13392–7
- [16] Palmer T, Sargent F and Berks B C 2005 Export of complex cofactor-containing proteins by the bacterial Tat pathway *Trends Microbiol.* **13** 175–80
- [17] Lindenstrauß U and Brüser T 2009 Tat transport of linker-containing proteins in *Escherichia coli* *FEMS Microbiol. Lett.* **295** 135–40
- [18] Richter S and Brüser T 2005 Targeting of unfolded PhoA to the TAT translocon of *Escherichia coli* *J. Biol. Chem.* **280** 42723–30
- [19] Whitaker N, Bageshwar U K and Musser S M 2012 Kinetics of precursor interactions with the bacterial Tat translocase detected by real-time FRET *J. Biol. Chem.* **287** 11252–60
- [20] Musser S M and Theg S M 2000 Characterization of the early steps of OE17 precursor transport by the thylakoid Δ pH/Tat machinery *Eur. J. Biochem.* **267** 2588–98
- [21] BageEshwar U K, Whitaker N, Liang F-C and Musser S M 2009 Interconvertibility of lipid- and translocon-bound forms of the bacterial Tat precursor pre-Sufl *Mol. Microbiol.* **74** 209–26
- [22] Lindenstrauß U, Matos C F R O, Graubner W, Robinson C and Brüser T 2010 Malformed recombinant Tat substrates are Tat-independently degraded in *Escherichia coli* *FEBS Lett.* **584** 3644–8
- [23] Alcock F, Baker M A B, Greene N P, Palmer T, Wallace M I and Berks B C 2013 Live cell imaging shows reversible assembly of the TatA component of the twin-arginine protein transport system *Proc. Natl. Acad. Sci. USA* **110** 3650–9
- [24] Tarry M J, Schäfer E, Chen S, Buchanan G, Greene N P, Lea S M, Palmer T, Saibil H R and Berks B C 2009 Structural analysis of substrate binding by the TatBC component of the twin-arginine protein transport system *Proc. Natl. Acad. Sci. USA* **106** 13284–9
- [25] Stanley N R, Palmer T and Berks B C 2000 The twin arginine consensus motif of Tat signal peptides is involved in Sec-independent protein targeting in *Escherichia coli* *J. Biol. Chem.* **275** 11591–6
- [26] Hinsley A P, Stanley N R, Palmer T and Berks B C 2001 A naturally occurring bacterial Tat signal peptide lacking one of the 'invariant' arginine residues of the consensus targeting motif *FEBS Lett.* **497** 45–49
- [27] Ma X and Cline K 2010 Multiple precursor proteins bind individual Tat receptor complexes and are collectively transported *EMBO J.* **29** 1477–88
- [28] Kostecki J S, Li H, Turner R J and DeLissa M P 2010 Visualizing interactions along the *Escherichia coli* twin-arginine translocation pathway using protein fragment complementation *PLOS One* **5** e9225
- [29] Gillespie D T 1977 Exact stochastic simulation of coupled chemical reactions *J. Phys. Chem.* **81** 2340–61
- [30] Zilman A, Di Talia S, Jovanovic-Taliman T, Chait B T, Rout M P and Magnasco M O 2010 Enhancement of transport selectivity through nano-channels by non-specific competition *PLoS Comput. Biol.* **6** e1000804
- [31] Berg O G and von Hippel P H 1985 Diffusion-controlled macromolecular interactions *Ann. Rev. Biophys. Biophys. Chem.* **14** 131–60
- [32] Howan K, Smith A J, Westblade L F, Joly N, Grange W, Zorman S, Darst S A, Savery N J and Strick T R 2012 Initiation of transcription-coupled repair characterized at single-molecule resolution *Nature* **490** 431–4
- [33] Dabney-Smith C, Mori H and Cline K 2006 Oligomers of Tha4 organize at the thylakoid Tat translocase during protein transport *J. Biol. Chem.* **281** 5476–83
- [34] Whitaker N, Bageshwar U and Musser S M 2013 Effect of cargo size and shape on the transport efficiency of the bacterial Tat translocase *FEBS Lett.* **587** 912–6
- [35] Müller M and Klösigen R B 2005 The Tat pathway in bacteria and chloroplasts *Mol. Membr. Biol.* **22** 113–21
- [36] Alder N N and Theg S M 2003 Energetics of protein transport across biological membranes: a study of the thylakoid Δ pH-dependent/cpTat pathway *Cell* **112** 231–42
- [37] Asai T, Shinoda Y, Nohara T, Yoshihisa T and Endo T 1999 Sec-dependent pathway and Δ pH-dependent pathway do not share a common translocation pore in thylakoidal protein transport *J. Biol. Chem.* **274** 20075–8
- [38] Antal T K, Kovalenko I B, Rubin A B and Tyystjärvi E 2013 Photosynthesis-related quantities for education and modeling *Photosynth. Res.* **117** 1–30
- [39] Jack R L, Buchanan G, Dubini A, Hatzixanthis K, Palmer T and Sargent F 2004 Coordinating assembly and export of complex bacterial proteins *EMBO J.* **23** 3962–72
- [40] Robinson C, Matos C F R O, Beck D, Ren C, Lawrence J, Vasisht N and Mendel S 2011 Transport and proofreading of proteins by the twin-arginine translocation (Tat) system in bacteria *Biochim. Biophys. Acta* **1808** 876–84